Acta Astronautica 176 (2020) 510–519

Contents lists available at ScienceDirect

Acta Astronautica

journal homepage: www.elsevier.com/locate/actaastro

Miniature docking mechanism for CubeSats☆

Francesco Branz [a,*], Lorenzo Olivieri [b], Francesco Sansone [c], Alessandro Francesconi [a]

[a] Department of Industrial Engineering, University of Padova, via Venezia 1, 35131 Padova, Italy
[b] Centre of Studies and Activities for Space "G. Colombo" – CISAS, University of Padova, via Venezia 15, 35131 Padova, Italy
[c] Stellar Project Srl, via Niccolò Tommaseo 69, 35131 Padova, Italy

ARTICLE INFO

Keywords:
CubeSat
Docking mechanisms
On-Orbit Servicing

ABSTRACT

This paper presents the design and characterization of a miniature docking mechanism for nanosatellites. Potential applications are several, including servicing of orbital vehicles (e.g. refuelling, components replacement, deorbiting or reboosting) and assembly of large structures (e.g. telescopes, antennas). The mechanism responds to the constant demand of enabling technologies from the booming small satellites market. The developed system has a traditional probe–drogue configuration; it is equipped with a sensor to detect contact and a single servo-actuator to lock the connection. The simple, though effective, design fills a relevant gap in the field of nanosatellite technologies. Numerical simulations have been conducted to evaluate the dynamics of docking procedures and to estimate loads exchanged at contact. Experimental results validate the simulations and prove the high tolerance to angular and linear (lateral) misalignment.

1. Introduction

Small satellites, especially those belonging to the nanosatellite (<10 kg) and microsatellite (<100 kg) class, are realizing a revolution in the space industry, thanks to their low cost and fast production time. The New Space Economy leverages on fleets or constellations of small satellites for applications that once were prerogative of much larger platforms, such as Earth observation and telecommunications. New satellite services of IoT and M2M based on global, low-latency coverage of the planet are also enabled by the use of multiple miniature spacecraft in LEO. On-Orbit Servicing (OOS) of client satellites, assembly of large structures in space (On-Orbit Assembly, OOA) and Active Debris Removal (ADR) are the most visionary applications and require significant technology advancements for their implementation, especially if small, autonomous spacecraft are employed. The literature provides several examples of OOS [1], OOA [2] and ADR [3–5] missions based on CubeSats.

Key enabling technologies are required to support these rapid changes in the space market. The most relevant developments currently under way involve micro-propulsion systems, high-throughput telecommunication terminals, guidance algorithms and navigation sensors, capture and servicing technologies. In particular, docking technologies that enable a miniature spacecraft to rigidly connect with another orbital vehicle (any size) are crucial for the majority of OOS and OOA mission scenarios, as they often foresee the presence of a smaller servicing vehicle that operates on a client system. In addition, it is common to develop down-scaled missions for technology demonstration purposes: proving docking between miniature autonomous vehicles can be of great value under such perspective.

The interest in docking technologies for small satellites is rather recent, with relevant work dating not earlier than the 2000s. Concepts based on different configurations have been proposed, which can be classified into three main categories: probe–drogue, androgynous, magnetic.

The probe–drogue configuration is possibly the simplest for docking systems, and has been adopted for large space vehicles since the 1960s. The Michigan Aerospace Autonomous Microsatellite Docking System prototype [6] belongs to this category. In the framework of the ARCADE student project, another docking system based on the probe–drogue configuration was developed at the University of Padova, Italy [7,8]. Besides the capability of creating a rigid connection between the two vehicles, the system also featured a soft docking functionality: an electromagnet was integrated in the drogue allowing to pull the probe during approach and to push it away during release manoeuvres.

The SPHERES project (Massachusetts Institute of Technology) produced one of the most advanced systems for autonomous rendezvous and docking manoeuvres conceived for small satellites [9]. The SPHERES vehicles feature the Universal Docking Port (UDP) [10], which is provided with a non-axial-symmetric androgynous docking

☆ This work is supported by University of Padova, Italy, project FRAN_SID16_02.
* Corresponding author.
E-mail address: francesco.branz@unipd.it (F. Branz).

https://doi.org/10.1016/j.actaastro.2020.06.042
Received 4 February 2020; Received in revised form 16 June 2020; Accepted 25 June 2020
Available online 2 July 2020

Nomenclature

ADR	Active Debris Removal
$ARCADE$	Autonomous Rendezvous Control And Docking Experiment
$ASSIST$	hArmonised System Study on Interfaces and Standardization of fuel Transfer
CAD	Computer Aided Design
$CPOD$	CubeSat Proximity Operations Demonstration
DoF	Degree of Freedom
GNC	Guidance, Navigation and Control
$iBOSS$	intelligent Building Blocks for On-Orbit Satellite
IOT	Internet of Things
IR	Infrared
$iSSI$	intelligent Space System Interface
LEO	Low Earth Orbit
$M2M$	Machine to Machine
OOA	On-Orbit Assembly
OOS	On-Orbit Servicing
$PACMAN$	Position and Attitude Control with MAgnetic Navigation for CubeSats
RVD	Rendezvous and Docking
$SPHERES$	Synchronized Position Hold Engage and Reorient Experimental Satellite
ToF	Time-of-Flight
UDP	Universal Docking Port

system and a relative navigation system comprising a miniature camera and a set of four visual markers. More recently, the CubeSat Proximity Operations Demonstration (CPOD) project developed an androgynous docking interface for 3 U CubeSats [11]. Each satellite is equipped with a standard axial-symmetric docking unit with three petals. The mechanism opens from the stowed configuration, while the spacecraft rotates along the axis of symmetry to align with the partner unit docking interface. The mechanism locks to the partner interface, realizing a rigid connection. A semi-androgynous docking system conceived for microsatellites was developed at the University of Padova [12]. It is based on a standard docking interface with morphing capabilities: during joining operations between two spacecraft, one interface morphs acting as a grasper and the other one acts as a handle.

Magnetic docking was also investigated in recent years. A few studies intended to provide control of relative dynamics of two approaching objects, but they did not address the development of hard-docking mechanisms. The Electro-Magnetic Kelvin Clamp Docking System [2], developed by Surrey Space Centre, Caltech and NASA Jet Propulsion Laboratory, comprises three probe–drogue interfaces provided with pulse-width modulated electromagnets for proximity operations and soft docking. Within the PACMAN project of the University of Padova [13], a 0.5 U package for proximity rendezvous and soft docking has been developed; it is based on four active electromagnets to perform close range rendezvous with an electromagnetic target or a twin interface.

Other studies focused on berthing interfaces to assemble modular systems with the assistance of robotic arms. The iSSI system, designed in the framework of German iBOSS program, consists in a multifunctional androgynous berthing interface with power, data, and thermal transfer capabilities [14]. Developed in the framework of ESA activities, the ASSIST interface consists in an integrated berthing mechanism with peripheral electrical, gas, liquid connectors, leak check systems, optical/radio markers for cooperative rendezvous [15].

In this paper, the authors present a miniaturized docking system specifically designed for CubeSat platforms. The system is compact, based on the probe–drogue configuration, features a minimum amount of actuations and moving parts, and is suitable for both cooperative and uncooperative docking manoeuvres, only requiring the target to be prepared by providing it with a passive drogue interface. The device is designed to fill the lack of solutions available for CubeSat-class vehicles, providing a simple system with minimal requirements to the host platform and a high tolerance to close range approach uncertainties on attitude, position, attitude rate and linear velocity. Also, numerical simulations and experimental results used to characterize the mechanism behaviour are presented, providing a more detailed description compared to what is generally available in the literature on comparable devices.

The remainder of the paper is organized as follows: Section 2 describes the docking device, the design drivers and the concept of operation; Section 3 presents the results of numerical simulations that were carried out in order to investigate the behaviour of the mechanism in dynamic conditions, with focus on the tolerance on angular and lateral misalignment; Section 4 presents the results of a test campaign aimed at the experimental validation of the numerical results and the mechanism concept; conclusions are drawn in Section 5.

2. Mechanism description

The reference scenario considered during the mechanism design considers a small service vehicle (CubeSat) that docks to a larger, prepared, passive orbital object. The quantitative results presented in this work are relevant for a scenario with a target-to-chaser mass ratio of 10 or more.

The docking mechanism main function is to provide a rigid connection between two satellites. It is designed with a geometry that facilitates final alignment and tolerates positioning errors due to limitations in the GNC subsystem performances. Simplicity is strongly pursued: actuators and moving parts are reduced to the minimum in order to limit failure risk; sensors are simple and easily made redundant.

2.1. Requirements

The docking mechanism design is driven by a number of requirements derived from a typical OOS mission scenario where a chaser CubeSat docks to a prepared, massive target object and performs some sort of servicing operations. In fact, the proposed design was not developed in the framework of a specific mission and, for the sake of generality, only one quantitative performance requirement is defined. The following requirements are identified:

R1 (functional) the system shall provide a rigid mechanical connection between two space vehicles, one acting as chaser and the other one as target;

R2 (functional) the chaser system shall be capable of realizing the connection even if the target vehicle is passive (i.e. non cooperative);

R3 (design) the envelope of the system protruding parts shall be contained within a cylindrical volume with diameter 64 mm and height of 36 mm, as specified by the 3 U+ CubeSat design standard (‘tuna can’ extra volume) [16];

R4 (performance) the system shall tolerate an angular misalignment greater than 1.5 deg and a lateral misalignment greater than 5 mm in order to guarantee compatibility of the docking mechanism with the relative attitude and position estimations provided by the relative navigation sensor developed by the authors in [17].

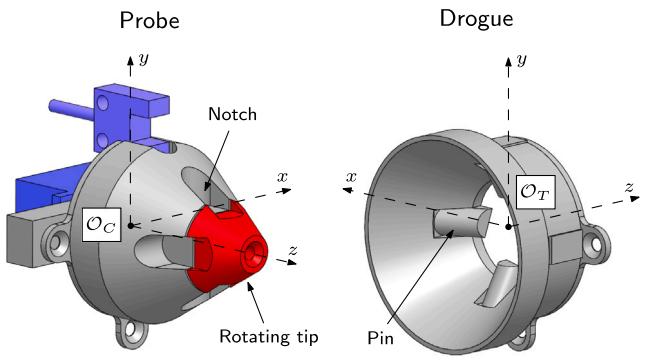

Fig. 1. 3D CAD drawing of the docking mechanism (with $\mathcal{O}_C$ and $\mathcal{O}_T$ frames of reference): static parts (grey), rotating parts (red), other devices (blue). (For interpretation of the references to colour in this figure legend, the reader is referred to the web version of this article.)

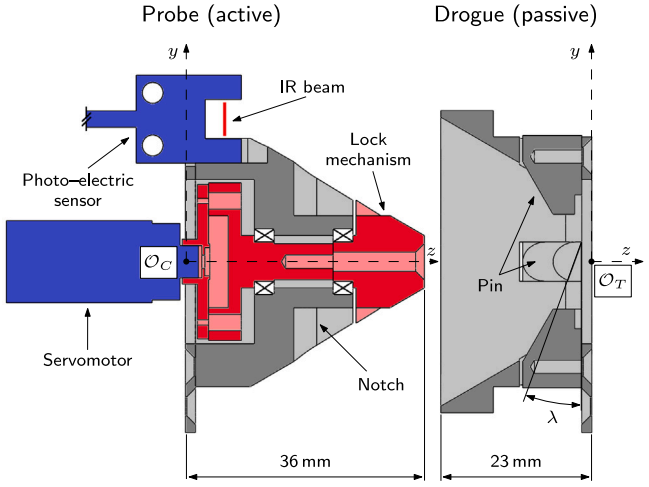

Fig. 2. Cross section of the docking mechanism (side view, yz plane, $+x$ direction) with static parts (grey), rotating parts (red) and other devices (blue). (For interpretation of the references to colour in this figure legend, the reader is referred to the web version of this article.)

2.2. System design

It is worth defining two frames of reference to consistently describe the mechanism design, working principle and validation scenarios (see Fig. 1). The first frame is fixed to the chaser body with origin $\mathcal{O}_C$ at the mechanical interface between the probe and the chaser body, with the xy plane coincident with the external surface of the vehicle (*chaser frame*); the second frame is fixed to the target body with origin $\mathcal{O}_T$ at the mechanical interface between the drogue and the target, with the xy plane coincident with the external surface of the target (*target frame*).

The mechanism adopts the traditional probe–drogue configuration, with an active probe and a passive drogue, as shown in Figs. 1 and 2. The active drogue has a conic shape, with a rotating tip used to lock the connection when docking is achieved. The probe is axial-symmetric around the z axis of the $\mathcal{O}_C$ frame. The passive drogue can be mounted on the external surface of any orbital object, with no need for power supply or control (R2), allowing to achieve uncooperative docking with a prepared target. The drogue is a static structure, shaped as an axial-symmetric, concave receptacle with four radial, 90-deg-spaced pins, which are inward oriented. The z axis of the $\mathcal{O}_T$ frame is the symmetry axis of the drogue. The drogue pins fit into notches in the probe case constraining the relative rotation around the mechanism axis of symmetry, z; they are engaged by the rotating tip when the mechanism is locked. The moving tip is actuated by a micro servomotor (Feetech FS90H) through a rod supported by ball bearings (Fig. 2, red). The servomotor positioning resolution is approximately 1.8 deg. When actuated, the rotating tip pushes against the back faces of the pins that are inclined by an angle $\lambda = 20\,\text{deg}$ w.r.t. the xy plane in the target frame (see Fig. 2). Similarly to what happens in screws, the servomotor torque is converted to axial force (see Fig. 3). Forces exchanged between the rotating tip and the static pins build up a docking axial preload estimated in the order of 20÷25 N, guaranteeing a rigid connection (R1). Preload estimation is based on simple geometrical considerations and on the nominal stall torque of the servomotor with some uncertainty on friction coefficient. Such high values of preload can be maintained only when the motor is actuated; when power supply is removed, preload is reduced. The nominal peak power consumption is <4 W. Contact between probe and drogue is detected by a photo-electric sensor (Panasonic PM–U25): when in the correct docking position, the drogue external rim interrupts the IR beam of the sensor and the locking signal is immediately transmitted to the servomotor. Commercial off-the-shelf components are adopted and integrated into in-house developed mechanical parts.

The probe and drogue protrude from the host spacecraft external surfaces by 36 mm and 23 mm respectively, while their external diameters are 38 mm and 46 mm respectively. These dimensions are compatible with the CubeSat standard if the docking interfaces are mounted on either (top or bottom) of the CubeSat bases (R3). A laboratory prototype was manufactured to perform the experiments described in this paper. The majority of the prototype components are made of plastic material, except for motion transmission components and supports that are machined in aluminium. The probe mass is 51 g including sensor and actuator, while the drogue mass is 17 g, for a total mass of 68 g. These mass values are only partially representative of a future flight model, which would probably be manufactured mainly in aluminium; given the mass densities of the two materials and accounting for some mass-oriented optimization, the total mass of a flight version of the docking mechanism is estimated to be below 150 g. The prototype is part of an integrated rendezvous and docking interface developed by the authors at the University of Padova. The interface features a vision-based navigation sensor for the determination of relative attitude and distance between target and chaser with an accuracy of ±1.5 deg and ±5 mm respectively [17].

2.3. Concept of operation

The sequence of operations is straightforward as a consequence of the extreme simplicity of the proposed design. Docking operations begin when proximity rendezvous is almost completed: the chaser vehicle is close to the target (i.e. less than 1 m, inside the relative navigation sensors range [18]), the docking interfaces are facing one another and relative velocity is low (i.e. less than 10 cm/s at 1 m), with the two spacecraft slowly moving closer to each other. The nominal sequence of events during a docking procedure is the following:

1. *Approach* — the chaser moves towards the target and the probe enters in the range of acceptance of the drogue.
2. *Contact* — the probe tip comes in contact with the drogue cavity and impact forces are exchanged between the interfaces.
3. *Insertion* — the probe slides into the drogue. Rebounds or discontinuous contacts can occur. Thrust from the chaser vehicle is useful at this time to counteract rebounds and overcome friction. Note that the target is assumed to be considerably more massive than the chaser vehicle and, therefore, the thrust provided is assumed to cause a negligible dynamic effect on the target.
4. *Self-alignment* — the shapes of drogue and probe force the vehicles to rotate and translate to achieve the correct alignment under the effect of the propulsion system. The interfaces are aligned if the rotation angles between the $\mathcal{O}_C$ and $\mathcal{O}_T$ frames are

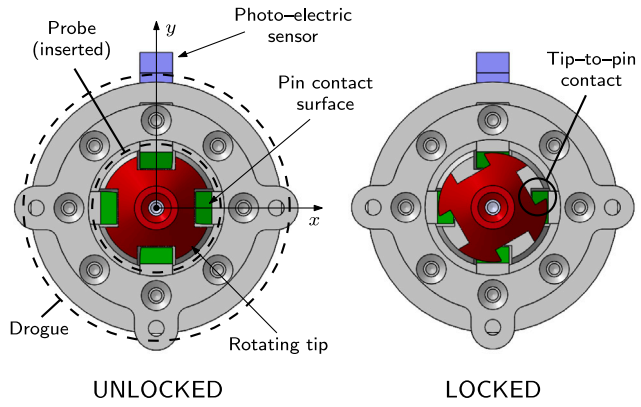

Fig. 3. Locking principle (mechanism view in $-z$ direction after full probe insertion): the tip (red) rotates and gets in contact with the inclined surface (green) of the pins, generating the axial preload force. (For interpretation of the references to colour in this figure legend, the reader is referred to the web version of this article.)

all zero (i.e. the rotation matrix is the identity matrix) and the z–axes of both frames are collinear. The geometry of the interfaces guarantees a considerable self-alignment range in pitch and yaw (up to ± 30 deg) and in lateral displacement (up to ± 30 mm, see Sections 3.1 and 4.1). Roll misalignment tolerance is limited by design to a few degrees (± 4 deg) due to the presence of the locking pins. However, the roll angle estimates provided by the vision-based sensor described in [17] are considerably more accurate than those for the pitch and yaw angles.

5. *Pins insertion* — when alignment is achieved, the drogue static pins slide into the probe notches and constrain rotation around the axis of symmetry of the docking mechanism (z).
6. *Docking detected* — the photo-electric sensor detects docking as soon as the probe is fully inserted in the drogue.
7. *Locking* — the servomotor rotates the probe tip, which engages the drogue static pins generating the axial load that guarantees a rigid connection (see Fig. 3).

The events described in the above sequence occur over a time span of $5 \div 15$ s, depending on initial approach speed, alignment conditions at first contact and thrust, as it was observed during the test campaign carried out on the low-friction table facility and described in Section 4.2.

3. Numerical simulations

Two sets of numerical simulations are performed to investigate the kinematic and dynamic behaviour of the docking system. The first set aims at the assessment of the docking mechanism operational range (kinematic simulation), while through the second one the loads exchanged during the docking procedure are evaluated (dynamic simulation).

3.1. Kinematic simulations

The docking mechanism operational range can be defined as a function of the maximum values of lateral and angular misalignment that still allow the docking procedure to succeed. From the kinematic point of view, these values depend only on the mechanism geometry and can be set as a preliminary constraint for rendezvous and docking GNC strategies.

Operational range is determined through a series of numerical simulations with different initial lateral and angular misalignment between probe and drogue. Simulations are performed with the MSC Adams multibody dynamics software. The geometrical model is directly

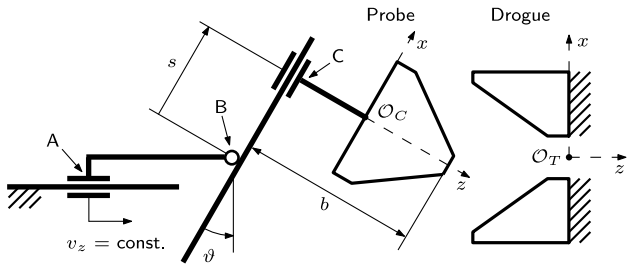

Fig. 4. Scheme of the kinematic simulation model and kinematic experiment setup (top view, xz plane, $-y$ direction).

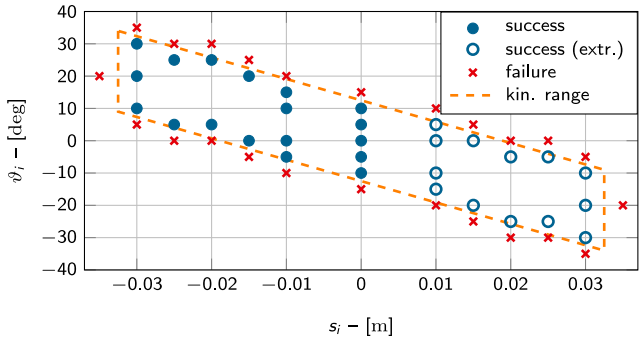

Fig. 5. Kinematic simulations results: initial alignment. Circles mark successful docking (if marker is empty, data point is extrapolated from symmetry considerations), crosses mark failed docking. The dashed line wraps the estimated kinematic range.

imported from the CAD reported in Fig. 1: it consists of five parts for the drogue (main body and four fixed pins) and two parts for the probe (main body and rotating tip). The drogue is held at a fixed position, while the probe is mounted on a frame approaching the drogue at a constant velocity, v_z (see Fig. 4). The symmetry axes of the interfaces are coplanar and lay on the xz horizontal plane, common to both reference frames; this assumption is valid in this paper for both simulations and experiments. The probe is constrained to the frame through a rotation joint (B) and a prismatic joint (C), allowing free rotation, ϑ, around the vertical axis, y, and free translation, s, along the horizontal direction, x (radial w.r.t. the docking mechanism axial symmetry). The distance, b, of the probe tip from the joint C is equal to 73 mm and it is slightly smaller than, but comparable to the distance (86 mm) between the tip and the vertical axis passing through the geometrical centre of the CubeSat mock-up used during dynamic tests (see Section 4.2); note that the kinematic range estimated here is a function of b and its validity is limited to the described geometrical configuration. Different initial lateral and angular misalignments are imposed and the mechanism capability to self-align and dock is evaluated.

A total number of 31 simulations have been performed in the first simulation campaign. Results are reported on a lateral vs. angular misalignment (s vs. ϑ) chart in Fig. 5: successful docking is marked with filled blue circles, while unsuccessful simulations are represented in red crosses. Due to symmetry considerations, results can be extrapolated for the rest of the operational range (empty blue circles). The orange dashed envelope wraps the expected operational kinematic range of the docking mechanism. For perfect lateral alignment, $s_i = 0$, the mechanism angular range is limited to approximately $\vartheta = \pm 12$ deg; for larger angles the probe tip position is placed outside the drogue cone, preventing a successful docking. Lateral misalignments influence the probe tip position with respect to the drogue centre and, therefore, the angular range shifts, while keeping the same amplitude. Simulations show that the maximum lateral misalignment is approximately ± 30 mm.

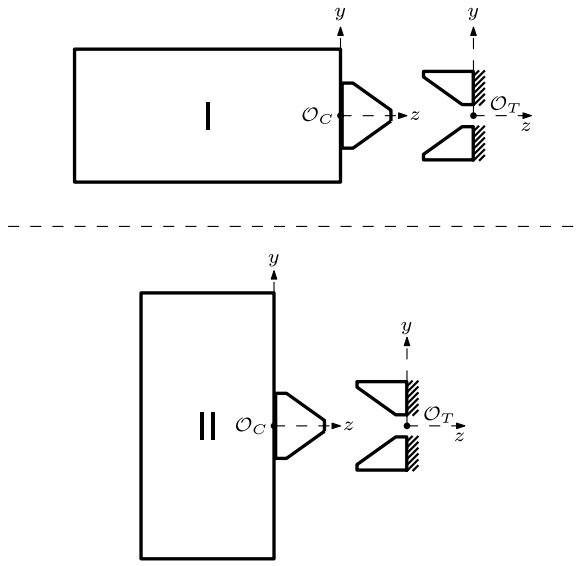

Fig. 6. Schematic representation of the two configurations considered for dynamic simulations (side view, yz plane, $+x$ direction).

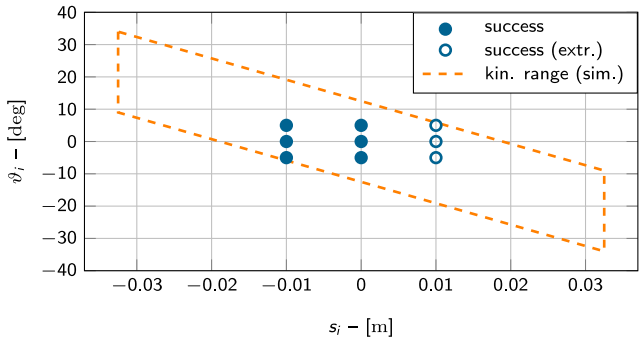

Fig. 7. Dynamic simulations results (configuration I): initial alignment. Circles mark successful docking (if marker is empty, data point is extrapolated from symmetry considerations). The dashed line wraps the kinematic range (see Fig. 5).

Table 1
Dynamic simulation results (configuration I): Impact loads at constant velocity (5 mm/s).

Misalignment		Loads		Misalignment		Loads	
s [mm]	ϑ [deg]	Force [N]	Torque [mN m]	s [mm]	ϑ [deg]	Force [N]	Torque [mN m]
−10	5	0.09	0.7	0	5	0.07	1.1
−10	0	0.06	1.0	0	0	0.08	0.4
−10	−5	0.09	0.8	0	−5	0.07	1.1

3.2. Dynamic simulations

The second type of simulations aims at understanding the loads exchanged during docking. In this case, a reduced workspace is investigated (limited to 10 mm and ±5 deg, compatible with state-of-the-art relative navigation sensors [17,18]). Again, simulations are performed with MSC Adams using geometries imported from CAD drawings. Two different configurations are simulated: the first one is representative of a realistic orbital scenario, while the second one better replicates the experimental setup used for dynamic tests (see Section 4.2). The main difference between the two configurations is the positioning of the docking mechanism on the chaser body. In the first case (I in Fig. 6), the mechanism is mounted on the square base of the CubeSat, i.e. the face perpendicular to the body major dimension; in the second case (II in Fig. 6), the mechanism is mounted on the lateral, longer side of the 2 U chaser. Another important difference between the two configurations is impact velocity. In configuration I, impact velocity is set to 5 mm/s, which is representative of a real orbital scenario and is in line with the *0.1%–rule* (more details are provided later in the text). Differently, in configuration II impact velocities are in the 15 −50 mm/s range, which is what is practically achievable with the dynamic experimental setup (see Section 4.2) due to the presence of residual friction and lack of velocity control. The dynamic range of configuration II also represents a more challenging scenario that allows to test the upper limits of the system capabilities.

The first set of simulations considers the I configuration. The probe is constrained to the square base of a dummy mass representative of a 2 U CubeSat and approaches a fixed drogue at a constant velocity (aligned with the probe symmetry axis z), and with different lateral and angular misalignments (see Table 1). No external force is applied to the system. For both probe and drogue the selected material is aluminium, while for the dummy CubeSat both mass and inertia have been calculated considering a mean density of 1000 kg/m^3. The contact force model is described in [19] and has the following form:

$$F = kd^{\mu} \tag{1}$$

where k is a constant depending on material, d is the local deformation of the impacting bodies and μ is the force coefficient. In this case $k = 10^8$ and $\mu = 2.2$ (aluminium). Docking is more challenging at high approach speed due to potential rebound. Hardly any standardized approach convention is available to determine the optimal velocity value. The *0.1%–rule* (approach speed below 0.1% of residual distance) was adopted by NASA for manual docking of large manned vehicles, but it is now considered excessively conservative [20]. The selected speed value is 5 mm/s, which corresponds to 0.5% of distance at 1 m.

Maximum contact loads for each misalignment condition are reported in Table 1. Exchanged forces and torques are always below or equal to 0.1 N and 1.1 mN m respectively for all configurations. Evaluating contact loads is important for assessing risks for the vehicles structural integrity and dynamic effects on the attitude. The presented load values are quite low, if compared to those presented in [12] (simulations: 3 N at an approach velocity of 2 mm/s; experiments: 2 N at 10 mm/s) for a mechanism about three times larger than the one proposed in this work.

A second set of dynamic simulations is performed to emulate the experimental conditions described in Section 4.2. In this case the probe is constrained to the geometric centre of a lateral face of the 2 U CubeSat dummy mass (2.3 kg), adopting the II configuration in Fig. 6. Two forces (each 0.01 N) push the CubeSat dummy towards the fixed drogue, emulating the action of the fans that equip the experimental mock-up, as depicted in Fig. 11: the forces are symmetric w.r.t. the yz plane and are applied to the centres of the $+x$ and $-x$ sides of the structure. This numerical simulation campaign allows to emulate the 3-DoF dynamics experiments, as the motion develops in the xz plane and the dummy mass inertia moment with respect to the y direction is equivalent to that of the experimental mock-up. Both probe and drogue are modelled considering a plastic material matching the characteristics of the prototype. With reference to the contact model in Eq. (1), the force coefficient is $\mu = 1.5$ and the equivalent stiffness is $k = 10^7$. Docking simulations are performed with four different approach velocities (15 mm/s, 25 mm/s, 35 mm/s and 50 mm/s at first contact) and different lateral (up to 1 mm) and angular (up to 5 deg) misalignments. Note that the simulated dynamic range in this case (configuration II) is reduced compared to the previous case (configuration I), to keep it closer to the actual range tested in dynamic tests.

In all simulated conditions the probe is able to self-align and reach the docking configuration. In order to ease the comparison between simulated and experimental results, the peak forces and impulses of the first probe-to-drogue contact are shown in Fig. 14 as a function of the contact velocity (i.e. velocity perpendicular to the contact surface).

Table 2
Dynamic simulation results (configuration II): Impact loads and impulse at constant misalignment (1 mm and 5 deg).

Velocity	Loads		Impulse
	Force	Torque	
[mm/s]	[N]	[N m]	[N s]
15	1.38	10.4	0.0104
25	2.45	16.7	0.0167
35	3.67	25.6	0.0232
50	5.68	39.6	0.0334

Among numerical simulation outputs, the impulse is less sensitive to configuration parameters (e.g. material characteristics, simulation time-step) and can be employed to estimate the momentum exchange during the impact; in any case, information on peak force is still relevant to assess the structural response of the mechanism. The peak contact force ranges between 1.4 N and 5.7 N, the peak torque ranges between 10 mN m and 40 mN m, while the impulse ranges between 0.01 N s and 0.033 N s; data on peak loads are summarized in Table 2.

4. Experimental validation

The proposed design and the numerical simulations are validated by means of laboratory experiments. Two different experiments are conceived: kinematic and dynamic tests. This section describes the experimental setup, procedure and results for both cases.

4.1. Kinematic experiment

Kinematic analysis is valuable to properly characterize the docking mechanism as a standalone device, regardless of the orbital system as a whole. The test objective is to evaluate the mechanism capability to tolerate misalignment and still achieve a successful docking, aiming at validating the proposed geometry and the numerical model used to estimate the system operational range presented in Section 3.1. The experiment neglects the effects of the forces exchanged between the docking interfaces and provides a design rule by measuring the maximum theoretical navigation error compatible with docking.

The kinematic scheme of the experimental setup replicates the kinematic conditions of the simulated model shown in Fig. 4, while Fig. 8 is a picture of the actual setup. The drogue is fixed to the laboratory table, while the probe is mounted on the moving platform of the 3-DoF motorized setup that is shown in Fig. 8. A stepper motor with worm rod pushes the platform (A in Fig. 4) towards the drogue at a constant velocity, v_z. On the platform, a rotating support (B) holds a horizontal linear guide with a cart (C) that is directly connected to the docking probe. Rotation, ϑ, around the vertical axis, y, and horizontal linear motion, s, along the x axis (radial w.r.t. the docking mechanism axial symmetry) are free. The actual distance b between the probe tip and the linear guide is 73 mm, with considerations similar to those made for the kinematic model used in simulations (see Section 3.1).

The test procedure starts with the probe at a distance of 50 mm from the drogue, with no engagement between the two, and stops as soon as the optical switch detects a complete docking. Linear and angular initial misalignment (s_i and ϑ_i) are manually imposed to the probe on joints B and C, and measured with a Time-of-Flight (ToF) distance sensor (STMicroelectronics VL6180X) and an optical encoder (Broadcomm HEDS–9100 encoder module and HEDS–5120 code-wheel). Static measurements show that the accuracy of the ToF sensor is ±1.2 mm (standard deviation), while its resolution is 1 mm. Collected data show that the encoder accuracy is comparable to its resolution and equal to ±0.18 deg. As contact occurs, the probe slides inside the drogue and alignment is achieved thanks to the mechanism geometry. In this experiment the probe rotating tip is not actuated, since the test objective is to validate only the self-alignment capabilities of the docking interfaces geometry; locking is verified with dynamic experiments (see Section 4.2). Different values of misalignment are tested to estimate the tolerance ranges of the mechanism.

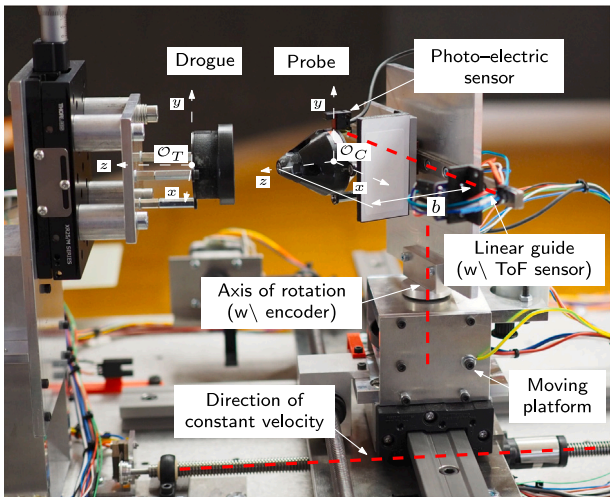

Fig. 8. Kinematic test setup with fixed drogue and probe installed on moving platform.

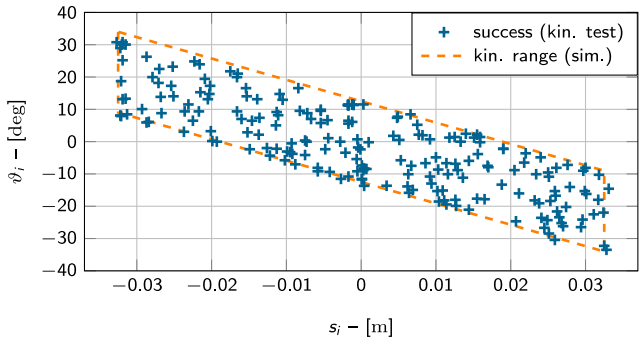

Fig. 9. Kinematic experiment results: alignment at first contact. The crosses (+) mark successful docking runs, the orange dashed line marks the kinematic envelope estimated with simulations (see Fig. 5).

In general, a docking procedure is considered successful if a safe and rigid connection between the interfaces is achieved. Since locking is not actuated during the kinematic tests, the success criterion adopted is the full insertion of the probe into the drogue as it is detected by the photo-electric sensor. Fig. 9 presents the initial contact conditions (s_i, ϑ_i) of 200 successful test runs, providing a complete understanding of the mechanism capability to withstand non-nominal approach conditions. Each cross marks an experimental point with different values of s_i and ϑ_i. The dashed line wraps the envelope of initial conditions that allow successful docking as estimated from simulations (see Section 3). All the presented experimental points have been chosen within the expected kinematic range, because operation outside such range may result in unsuccessful docking and potential damage to the experimental setup.

When successful insertion is achieved and full contact between the interfaces is detected by the photo-electric sensor, the final values s_f and ϑ_f are nominally null. Nevertheless, the design allows for some tolerance in the actual final values, to cope with manufacturing and assembly uncertainties. The measured values of s_f and ϑ_f fall within an interval of ±2 mm and ±0.2 deg respectively in more than 90% of cases. These values are comparable to the sensors resolutions, allowing to speculate whether the true values could be smaller. In any case, measuring the residual misalignments with a better accuracy is beyond the scope of this work, since they fall within the mechanism design tolerances and are compatible with the locking tip actuation.

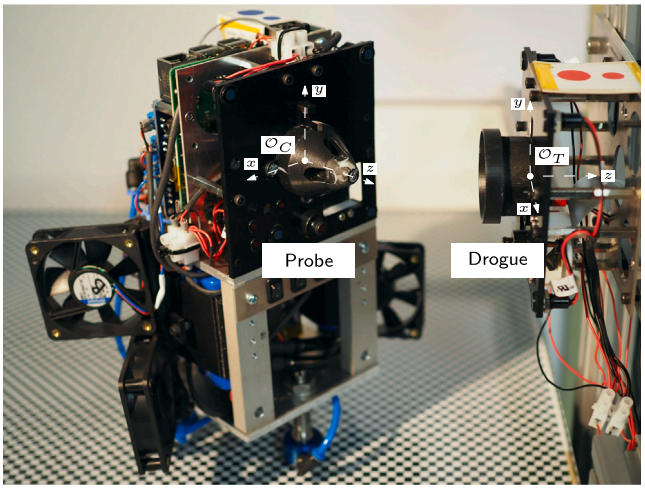

Fig. 10. Docking interfaces mounted on the CubeSat mock-up (probe) and fixed support (drogue) for dynamic testing.

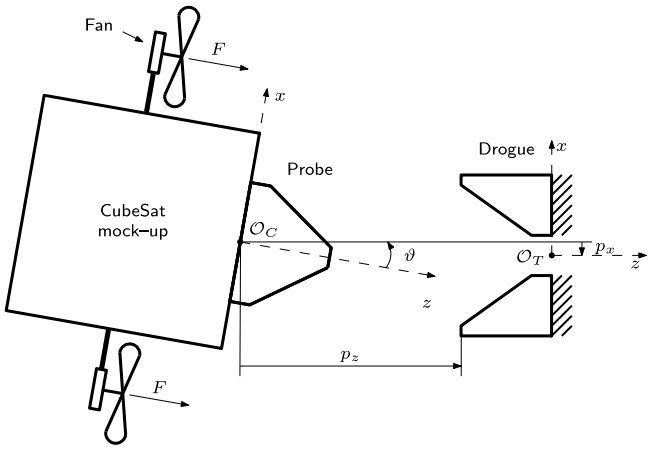

Fig. 11. Scheme of the flat table dynamic experiment (top view, xz plane, $-y$ direction).

4.2. Dynamic experiment

The experiment described in Section 4.1 is useful to determine the kinematic limits of the proposed mechanism geometry, but fails to verify the mechanism functionality in relevant dynamic conditions. In the kinematic test, the mechanism probe is constrained to a rigidly moving platform and pushed at constant velocity towards the drogue: motion is partially restricted and the dynamic effects of mass, inertia and contact forces are removed. In order to study the dynamics of docking in realistic conditions, a flat table experiment has been developed, with the probe interface mounted on a nanosatellite mock-up and the drogue fixed to a rigid structure. Fig. 10 shows the two docking interfaces integrated in the dynamic test setup. The proposed experiment is intended to verify the mechanism functionality when mounted on a free moving vehicle and emulates the scenario where a nanosatellite chases a much larger spacecraft.

Unsuccessful docking is often due to excessive contact forces that can lead to rebound or jamming. Forces are a function of dynamic parameters (e.g. mass and inertia) and, therefore, they are strongly dependent on the characteristics of the joining vehicles. The presented dynamic test, although significant for a wide range of OOS mission scenarios, provides results limited to the case where a small vehicle docks to a larger platform. Nevertheless, the dynamic test validates the mechanism functionality and provides a valuable benchmark for advanced designs and future developments.

Fig. 11 is a schematic drawing of the dynamic experiment setup. The mechanism probe is mounted on the side of a 2 U CubeSat mock-up that is free to move on the glass surface of a flat table, while the drogue is fixed to a rigid support, directly connected to the flat table structure. The fixed target structure is dynamically equivalent to a free object with infinite mass and inertia. It is considered a reasonable approximation of the dynamic behaviour of a target satellite at least one order of magnitude heavier than the chaser (target-to-chaser mass ratio of 10 or more). The CubeSat mock-up structure resembles a tall parallelepiped (10 cm × 10 cm × 20 cm) with a square basis (i.e. two 1 U blocks mounted one on top of the other along the vertical axis), with a total mass of 2.3 kg. Examples of this geometrical configuration (II in Fig. 6) can be found in the literature [2]. However, considering a 2 U or 3 U spacecraft, the I layout is more common and justified by the extra volume available in the 3 U+ CubeSat design standard [16], which allows for mounting the docking mechanism on the top face, i.e. on the plane normal to the main axis of the vehicle. The II configuration was chosen following considerations on the laboratory facility design, as the test setup is conceived to be part of a low-gravity simulator with the goal to perform testing of close-proximity operation procedures with a wider perspective. In this framework, the vertical configuration of the mock-up maximizes work-space and mobility on a finite flat table, proving advantageous. The limitations on the system representativeness of the II configuration are not negligible and accounted for by performing the simulations described in Section 3.2. The experimental results are used as a validation of the simulation models in the II configuration. The difference between the simulation models of configuration I, which is more representative of a realistic orbital scenario, and configuration II consists only in the inertial characteristics of the system. Therefore, the laboratory validation of configuration II is considered sufficient to validate also configuration I. As a result, the experiments are considered representative of a realistic docking scenario in orbit.

The vehicle is equipped with a pneumatic system that feeds three flat air-bearings (New Way Air Bearings S102501) from a disposable CO_2 cartridge (Lezyne). The CubeSat mock-up floats on a gas cushion that virtually removes friction. The vehicle motion is constrained to the horizontal plane having three DoFs: two translations in the plane (xz) and one rotation around the vertical axis (y). The mock-up is pushed towards the fixed docking interface by a set of fans (epm-pabst 605F–RS0) that are operated at a constant speed. The fans emulate a low-thrust propulsion system and generate a total force of 40 mN approximately (value computed from data collected through experimental characterization of the fans).

Relative position and attitude between the chaser and the target are measured by means of a vision system based on a commercial webcam (Logitech C270) that monitors the scene from above. The docking interfaces are equipped with optical markers that are detected through image analysis. Relative position and orientation between the markers is reconstructed by a dedicated algorithm. Statistical analysis shows that the measurement error is below 0.2 mm in position (standard deviation) and 0.25 deg in rotation (standard deviation). The measurements are employed to monitor the dynamic behaviour of the system and no closed-loop motion control is implemented in the experiment.

Fig. 12 presents the result of a test run. Curves show the relative trajectory between chaser and target in all three DoFs as measured in the $\mathcal{O}_T$ frame shown in Fig. 11: lateral displacement, p_x, relative distance, p_z, and angular misalignment, ϑ. The test runs for 10 s and notable instants are marked with capital letters (A, B, C, D, E). Starting at a distance of approximately 100 mm (between the chaser and target frames), from A to B the chaser approaches the target and the probe enters the drogue cavity. Approximately four seconds after the beginning of the run, first contact (C) occurs between the probe tip and the drogue. Up until first contact the CubeSat rotates around the y axis due to unbalanced thrust from the fans. After C the rotation

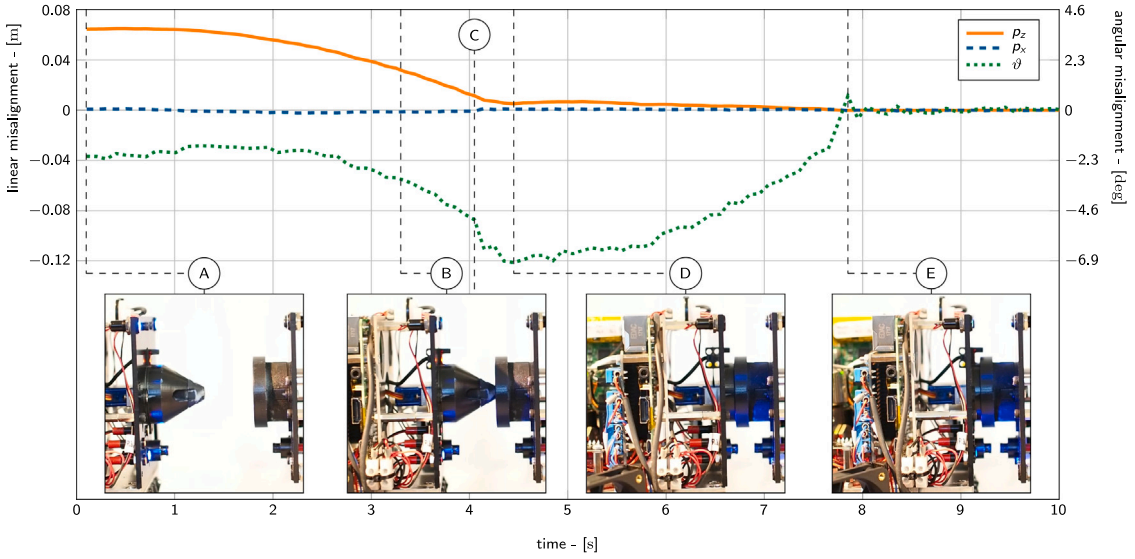

Fig. 12. Result of an example test run. Trajectory is described by the evolution of relative lateral position (p_x), distance (p_z) and angle (ϑ) over time. Five notable time instants are marked by capital letters (A, B, C, D, E) and corresponding video frames (side-view) are shown.

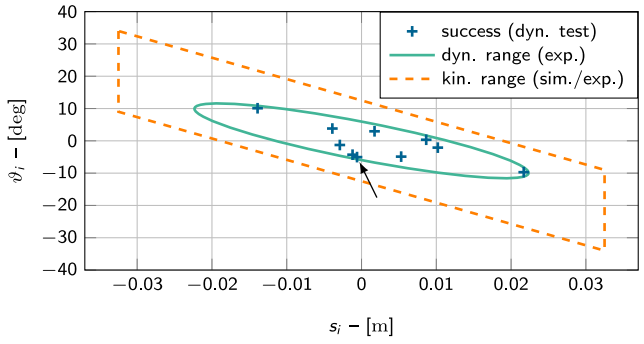

Fig. 13. Dynamic experiment results: alignment at first contact. The crosses (+) mark successful docking runs, the green ellipse encloses the measured dynamic range, the orange dashed line marks the kinematic envelope estimated with simulations (see Fig. 5), the black arrow identifies the data point relative to the example test detailed in Fig. 12.

changes due to contact forces. Less than a half-second later (D) a small rebound moves the chaser backwards by a few millimetres (orange solid line at 5 s). Relative velocity at contact (in the $+z$ direction of the $\mathcal{O}_T$ frame) is estimated via numerical derivative to be 29 mm/s. Between D and E, the constant thrust provided by the fans allows the mechanism to self-align and forces the probe to completely enter inside the drogue. At time instant E insertion and alignment are completed, docking is confirmed and the servomotor locks the connection. Some vibrations are exchanged between the interfaces as a consequence of the mechanism actuation, but oscillations are damped in approximately one second. Rigid connection is achieved and the docking procedure is complete.

The presented test run is successful and almost ideal. In some cases, the docking procedure is less smooth and multiple rebounds occur before alignment and insertion are completed. Nevertheless, the performed test campaign allowed to verify the mechanism functionality in several different conditions. Fig. 13 reports the alignment conditions at first contact in 10 successful test runs (the black arrow shows the experimental point relative to the example test described in Fig. 12). These results allow to draw the dynamic range (green ellipse) for the docking mechanism in the considered case of a 2 U CubeSat chasing a much larger spacecraft. The ellipse is the boundary of the minimum dynamic range, since the available experimental results do not allow to prove a wider range, although it is possible in theory. Therefore, the dynamic range is a subset of the kinematic range (dashed orange envelope) estimated through simulations (Fig. 7) and validated by kinematic tests (Fig. 9). The docking mechanism is proven capable to withstand a maximum lateral displacement greater than ±20 mm (at $|\vartheta_i| = 10$ deg) and an angular misalignment greater then ±5 deg (at $|s_i| = 0$ mm). The accuracy of navigation sensors is well below these values (R4). The mean velocity at first contact in the $+z$ direction of the $\mathcal{O}_T$ frame is 24 mm/s, with a minimum of 13 mm/s and a maximum of 42 mm/s. The velocity variability among single test runs is considerable, proving the robustness of the proposed design under diverse approach conditions.

Impact forces exchanged between the target drogue and the chaser probe have been estimated for six successful test runs. The chaser position and velocity (linear and angular) at the moment of first contact between probe tip and drogue have been extracted from data provided by the vision system used to monitor the experiment. A simulation tool has been developed to estimate the impact force at the first contact, considering the impact as perfectly elastic. This assumption is considered reasonable since no significant variation of total kinetic energy of the chaser can be inferred by the data provided by the camera. The equations of motion of the chaser vehicle are integrated through time starting from the position and velocity at the instant of first contact; the contact model is described by Eq. (1) and the parameters values are set in accordance with the simulations described in Section 3.2 ($k = 10^7$, $\mu = 1.5$), considering that the structural elements of the mechanism prototype are made of plastic. The penetration depth d is calculated at every instant and from Eq. (1) the resulting elastic force due to probe penetration is computed. The calculated maximum penetration depth is between 4×10^{-5} m and 8×10^{-5} m. The impulse is simply calculated by definition as the integral of the impact force through time, considering only the time steps when penetration actually occurs. The impulse duration is the time interval between the instant of first contact and the instant when the probe is no more in contact with the probe because of the repelling elastic force of the probe; impulse duration is typically $5 \div 10$ ms. The resulting impact peak force and the impulse exchanged by target and chaser at the first contact are presented in Fig. 14. The impact velocity, i.e. the component of the probe tip velocity vector

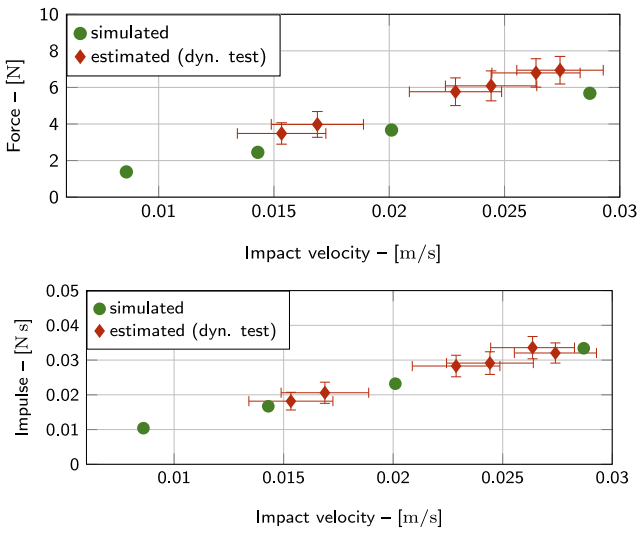

Fig. 14. Impact forces (top) and impulses (bottom): simulated (green dots) and estimated from dynamic test trajectories (red diamonds with error bars).

orthogonal to the drogue internal surface, varies between 15 mm/s and 28 mm/s, with uncertainty of ±2 mm/s (standard deviation). The peak impact force ranges between 3.5 N and 7.0 N (±0.7 N, standard deviation), while the first impact impulse is between 18×10^{-3} N s and 34×10^{-3} N s ($\pm 2 \times 10^{-3}$ N s, standard deviation). While not negligible, these peak force values do not pose a serious threat to the vehicles integrity. More relevant in a motion control perspective is the impulse, which is very low and easily manageable by the chaser attitude and orbital control systems. The results obtained with the described analysis are in good accordance with those provided by the dynamic simulations presented in Section 3.2 and reported in Fig. 14: the mean absolute error between the experiment and the simulation results is 1.34 N for impact force (relative error 24%) and 3.6×10^{-4} N s for impulse (relative error 1.4%).

5. Conclusions

This work describes the design and functionality of a miniature docking mechanism tailored for nanosatellites and compatible with the common CubeSat standard. Technologies to enable autonomous rendezvous and docking between small satellites are becoming more and more appealing as the market of miniature orbital platforms is growing rapidly with many profitable scenarios involving multiple independent agents.

This work provides a detailed description and experimental validation of a simple, yet effective, solution to the docking problem. The probe–drogue configuration is adopted for the proposed mechanism. It is equipped with a single actuator integrated in the active probe; a sensor detects docking. Actuation and sensing features allow to achieve a safe and rigid connection between the involved vehicles. Numerical simulations are presented to estimate the operational range of the mechanism in terms of lateral and angular misalignment. Kinematic and dynamic experiments are conducted to validate the simulation sets and to verify the mechanism behaviour within relevant boundary conditions. Experiment results confirm the simulation results, by proving the mechanism functionality in the considered misalignment ranges. Impact forces and impulses estimated from experiments are close to those obtained from simulations (mean force error: 1.34 N or 24%, mean impulse error: 3.6×10^{-4} N s or 1.4%).

The proposed mechanism contributes to the state of the art by filling a technological gap and providing validated figures useful to define mission requirements, although the work originates from a basic mission architecture that inevitably limits the generality of the results. The baseline scenario adopted features a small servicing chaser that docks to a larger vehicle. This is a reasonable working hypothesis, but more general cases (e.g. CubeSat-to-CubeSat RVD) are worth to be investigated as future analysis. The presented results allow to draw some preliminary considerations regarding the case of docking between two vehicles of comparable size: peak impact forces are expected to be lower, but rebounds could be more relevant; a reduced tolerance to relative velocities at contact is expected; on one side, the reduced inertia of the target improves its mobility easing the self-alignment between the docking interfaces, while, on the other side, reduces the attitude stability, making the docking procedures more challenging. In the case both the chaser and target vehicles are controlled and cooperate to achieve docking, the scenario changes considerably and most of the drawbacks highlighted above are mitigated.

Another strong hypothesis considered in the baseline scenario is the requirement for thrust provided by the chaser bus. Again, this appears to be an acceptable requirement for the majority of RVD missions, but future developments should consider the possibility that a continuous and adjustable thrust may be unavailable, at least in non-nominal conditions. The dynamic simulations (I) described in Section 3.2 show that docking without external forces is possible. Nevertheless, the results of this work support the argument that a lack of thrust could lead to difficulties in the full probe–drogue insertion, as rebounds and friction are not compensated.

Potential future developments include a deeper investigation of the contact dynamics during docking procedures and a detailed analysis of a realistic 3D docking scenario through both simulations and experiments.

Declaration of competing interest

The authors declare that they have no known competing financial interests or personal relationships that could have appeared to influence the work reported in this paper.

References

[1] A. Nanjangud, P. Blacker, S. Bandyopadhyay, Y. Gao, Robotics and AI-enabled on-orbit operations with future generation of small satellites, Proc. IEEE 106 (3) (2018) 429–439.
[2] C. Underwood, S. Pellegrino, V.J. Lappas, C.P. Bridges, J. Baker, Using CubeSat/micro-satellite technology to demonstrate the Autonomous Assembly of a Reconfigurable Space Telescope (AAReST), Acta Astronaut. 114 (2015) 112–122.
[3] B. Larbi, B. Grzesik, J. Radtke, C. Trentlage, E. Stoll, Active debris removal for mega constellations: CubeSat possible?, in: 9th International Workshop on Satellite Constellations and Formation Flying, Boulder, CO, USA, 2017, pp. 19–21.
[4] H. Hakima, M.C. Bazzocchi, M. Emami, A deorbiter cubesat for active orbital debris removal, Adv. Space Res. 61 (9) (2018) 2377–2392.
[5] C. Pirat, M. Richard-Noca, C. Paccolat, F. Belloni, R. Wiesendanger, D. Courtney, R. Walker, V. Gass, Mission design and GNC for in-orbit demonstration of active debris removal technologies with cubesats, Acta Astronaut. 130 (2017) 114–127.
[6] P. Tchoryk Jr., A.B. Hays, J.C. Pavlich, A docking solution for on-orbit satellite servicing: part of the responsive space equation, AIAA-LA Section/SSTC 2001 (2003) 1–3.
[7] A. Boesso, A. Francesconi, ARCADE small–scale docking mechanism for micro-satellites, Acta Astronaut. 86 (2013) 77–87.
[8] M. Barbetta, A. Boesso, F. Branz, A. Carron, L. Olivieri, J. Prendin, G. Rodeghiero, F. Sansone, L. Savioli, F. Spinello, et al., ARCADE–R2 Experiment on board BEXUS 17 stratospheric balloon, CEAS Space J. 7 (3) (2015) 347–358.
[9] S. Mohan, A. Saenz-Otero, S. Nolet, D.W. Miller, S. Sell, SPHERES Flight operations testing and execution, Acta Astronaut. 65 (7) (2009) 1121–1132.
[10] L. Rodgers, N. Hoff, E. Jordan, M. Heiman, D. Miller, A universal interface for modular spacecraft, in: 19th Annual AIAA/USU Conference on Small Satellites, 2005.
[11] J. Bowen, M. Villa, A. Williams, CubeSat based rendezvous, proximity operations, and docking in the CPOD mission, in: 29th Annual AIAA/USU Conference on Small Satellites, 2015.
[12] L. Olivieri, A. Francesconi, Design and test of a semiandrogynous docking mechanism for small satellites, Acta Astronaut. 122 (2016) 219–230.

[13] M. Duzzi, R. Casagrande, M. Mazzucato, F. Trevisi, F. Vitellino, M. Vitturi, A. Cenedese, A. Francesconi, Electromagnetic position and attitude control for PACMAN experiment, in: 10th International ESA Conference on Guidance, Navigation & Control Systems, Salzburg, Austria, 2017, vol. 29.
[14] M. Kortman, S. Ruhl, J. Weise, J. Kreisel, T. Schervan, H. Schmidt, A. Dafnis, Building block based iBoss approach: fully modular systems with standard interface to enhance future satellites, in: 66th International Astronautical Congress, Jersualem, Israel, 2015.
[15] A. Medina, A. Tomassini, M. Suatoni, M. Avilés, N. Solway, I. Coxhill, I.S. Paraskevas, G. Rekleitis, E. Papadopoulos, R. Krenn, et al., Towards a standardized grasping and refuelling on-orbit servicing for GEO spacecraft, Acta Astronaut. 134 (2017) 1–10.
[16] California Polytechnic State University, CubeSat Design Specifications, https://static1.squarespace.com/static/5418c831e4b0fa4ecac1bacd/t/56e9b62337013b6c063a655a/1458157095454/cds_rev13_final2.pdf.
[17] F. Sansone, F. Branz, A. Francesconi, A relative navigation sensor for CubeSats based on LED fiducial markers, Acta Astronaut. 146 (2018) 206–215.
[18] F. Sansone, L. Olivieri, F. Branz, A. Francesconi, Proximity relative navigation sensors for small-scale spacecraft and drones, in: 66th International Astronautical Congress, Jersualem, Israel, vol. 11, 2015, pp. 8261–8270.
[19] K.L. Johnson, Contact Mechanics, Cambridge University Press, 1987.
[20] A.R. Brody, Evaluation of the '0.1 percent rule' for docking maneuvers, J. Spacecr. Rockets 27 (1) (1990) 7–8.

Francesco Branz is a lecturer in Attitude Control of Satellites and Aircraft Systems at the Dept. of Industrial Engineering, University of Padova, Italy. He received his Ph.D. in 2016 at the Center of Studies and Activities for Space "G. Colombo" (CISAS) of the University of Padova with a thesis on modelling and control of dielectric elastomer actuators for space robotics. His research later focused on CubeSat technologies for attitude simulation and control, close range relative navigation and docking systems.

Lorenzo Olivieri received a Ph.D. in Measures for Space from the University of Padova in 2015 with a thesis on docking technologies for small spacecraft. His research interests include small satellites technologies, docking systems and capturing strategies and debris protection and removal. He is working as postdoctoral fellow at the Center for Space Studies "G. Colombo" (CISAS), University of Padova, Italy.

Francesco Sansone is system engineer at Stellar Project. He has a Ph.D. in Space Science and Technology from the Centre of Studies and Activities for Space "G. Colombo" (CISAS) of the University of Padova. His research and professional activities are in the field of systems and technologies for enhancing the capabilities of nanosatellites. This includes laser communication and relative navigation systems. He participated to and supported several research and student projects testing critical technologies in low-gravity environment. Francesco is co-inventor of the LaserCube stabilization and pointing subsystem and lead engineer for the development of the LaserCube terminal.

Alessandro Francesconi is associate professor of Space Systems at University of Padova, Italy. His main research topics are related to spacecraft systems and miniature satellites (with focus on on-orbit servicing, docking and capture of non-cooperative spacecraft, and laser communication), and space debris (where he has 20+ years of experience in studying hypervelocity impacts, satellites collisions and fragmentation). He has been chairman of the Protection Working Group of the Inter Agency Debris Coordination Committee, and he is member of the IAA Permanent Committee on Space Debris. He is co-founder of Stellar Project srl and co-inventor of the LaserCube stabilization and pointing subsystem.